ACS NANO

www.acsnano.org

ARTICLE

Valley Polarized Holes Induced Exciton Polaron Valley Splitting

Yueh-Chun Wu, Takashi Taniguchi, Kenji Watanabe, and Jun Yan*

Cite This: *ACS Nano* 2023, 17, 15641−15647

Read Online

ACCESS | Metrics & More | Article Recommendations | Supporting Information

ABSTRACT: **Monolayer transition metal dichalcogenide semiconductors are promising valleytronic materials. Among various quasi-particle excitations hosted by the system, the valley polarized holes are particularly interesting due to their long valley lifetime preserved by the large spin−orbit splitting and spin−valley locking in the valence band. Here we report that in the absence of any magnetic field a surprising valley splitting of exciton polarons can be induced by such valley polarized holes in monolayer WSe_2. The size of the splitting is comparable to that of the Zeeman effect in a magnetic field as high as 7 T and offers a quantitative approach to extract the hole density imbalance between the two valleys. We find that the density difference can easily achieve more than 10^{11} per cm^2, and it is tunable by gate voltage as well as optical excitation power. Our study highlights the response of exciton polarons to optical pumping and advances understanding of valley dependent phenomena in monolayer transition metal dichalcogenide.**

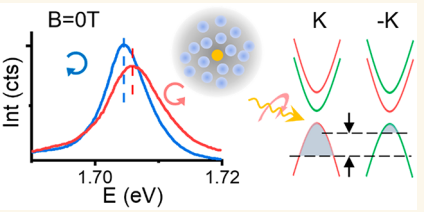

KEYWORDS: *2D materials, tungsten diselenide, exciton polaron, valley, spin*

The manipulation of the valley degree of freedom, a pseudospin, has attracted significant interest in the field of two-dimensional (2D) materials in recent years. In monolayer transition metal dichalcogenide (TMD) semiconductors, such as MoS_2 and WSe_2, energetically degenerate particles located at the two inequivalent valleys carry opposite spin, momentum, angular momentum, and magnetic dipole moment, offering a versatile means to address the valley pseudospin.[1] Time-reversal-symmetry breaking optical and magnetic fields have distinct impacts on quasi-particles residing in the two valleys and lead to rich valley phenomena. Well-known are optical generation of exciton valley polarization[2−11] and magnetic lifting of the valley degeneracy.[12−18] Further studies reveal that intense subgap optical fields can also break valley degeneracy via the optical Stark effect[19,20] and that circularly polarized photons generate not only valley polarized excitonic species but also valley polarized resident charges.[21−26] The valley polarized charges have orders of magnitude longer valley lifetimes compared to excitons, promising for future valleytronic devices. In electron doped TMDs, it was revealed that optical pumping can produce highly polarized resident electrons that give rise to opposite valley polarization for singlet and triplet trions.[27] Valley polarized holes are potentially even more interesting: Kerr rotation measurements indicate that these holes have longer valley lifetimes than the resident electrons, and unlike resident electrons, the valley polarized holes are highly robust against in-plane magnetic fields due to large spin−orbit splitting in the valence band.[21−25] However, other than lifetime measurements,[21−26] it has been challenging to perform quantitative assessment of the valley polarized holes, including basic questions such as the hole density difference between the two valleys and how it evolves with photon fluence and gate induced charge doping.

In this work, we excited hole-doped monolayer WSe_2 with circularly polarized photons and observed, in the absence of any magnetic field, a surprising energy splitting between the attractive exciton polarons residing in the two opposite valleys. To bring the valley polarons back to the same energy, a magnetic field as high as 7 T needs to be applied. Our analyses show that this interesting phenomenon is caused by valley polarized resident holes that were generated optically. Unlike pulsed excitations used in pump−probe studies of the transient optical Stark effect,[19,20] our experiment uses low-intensity continuous-wave (cw) optical illumination, which builds up valley polarized holes that compete with intervalley scattering and give rise to a persistent splitting. This persistent splitting provides an avenue to extract quantitatively the hole density difference between the two valleys, which is found to be a few times 10^{11} cm^{-2} depending upon the total hole density in the device. Our study also provides fresh insight into energy

Received: March 25, 2023
Accepted: July 26, 2023
Published: August 1, 2023

https://doi.org/10.1021/acsnano.3c02737
ACS Nano 2023, 17, 15641−15647

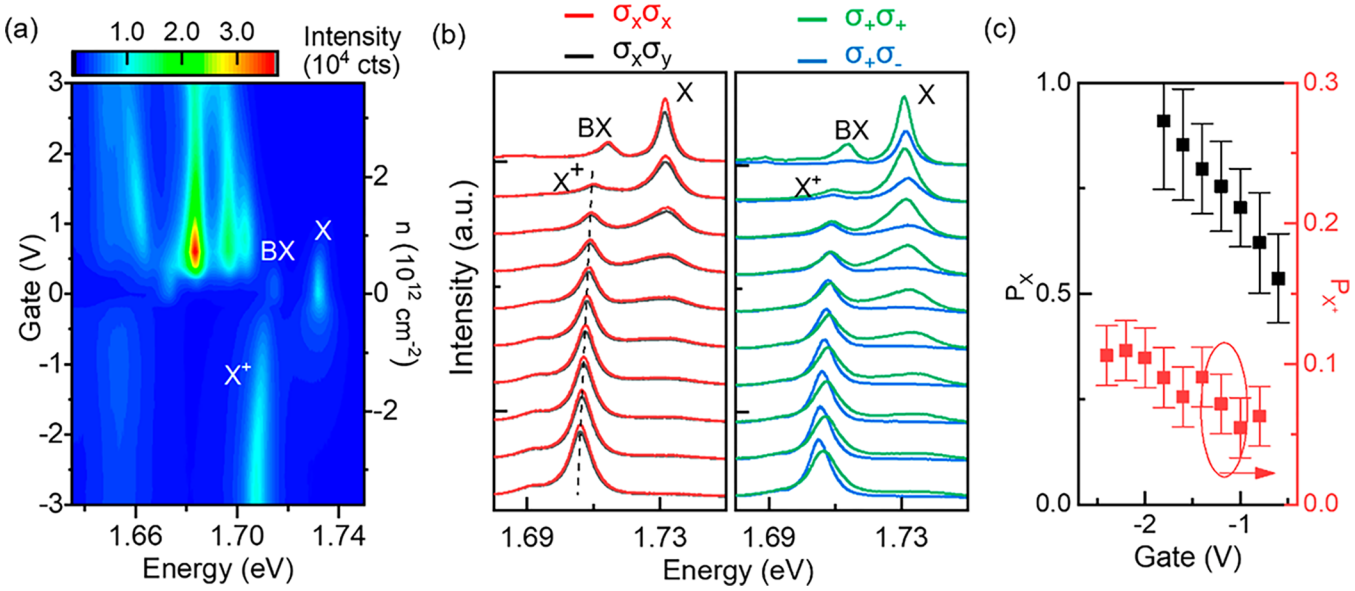

Figure 1. (a) False color map of gate voltage dependent 1L-WSe_2 photoluminescence excited by linearly polarized light. (b) Linear polarization resolved (left) and circular polarization resolved (right) spectra from V_g = 0 V (top) to V_g = −1.8 V (bottom). (c) Valley polarization of X and X^+ from the circular polarization resolved spectra in (b).

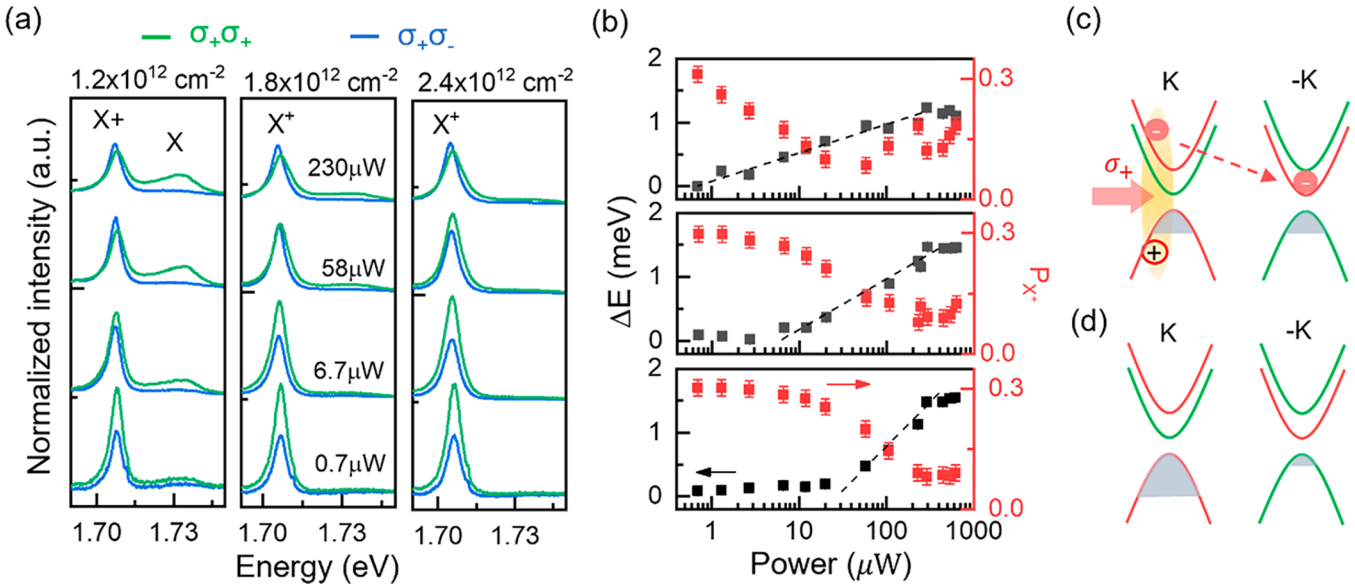

Figure 2. (a) Excitation-power-dependent photoluminescence spectra at various hole doping concentrations. The incident light has σ_+ circular polarization. The spectral intensity is normalized to incident power and integration time. (b) Excitation power-dependent energy splitting (black) and valley polarization (red) of X^+. From top to bottom: 1.2 × 10^{12}, 1.8 × 10^{12}, and 2.4 × 10^{12} cm^{-2}. The valley polarization is computed by comparing the integrated spectral area of emissions. (c, d) Schematic of light-induced imbalance of the hole Fermi sea between K and −K valleys.

splitting of excitonic modes for doped TMDs in an external magnetic field, a phenomenon widely interpreted only with the Zeeman effect arising from particles' magnetic dipole moments.

RESULTS

The monolayer WSe_2 devices (D1, D2) are encapsulated by hBN, and charge doping is achieved via the application of voltage to a graphene back gate. We examine the gate dependent photoluminescence of the devices at 4 K excited by a 633 nm He−Ne laser excitation. (Data presented are taken with device D1 unless otherwise stated.) As shown in Figure 1a, at the charge neutrality around V_g = 0 V, neutral exciton X and the four-particle biexciton BX can be identified at 1.731 and 1.714 eV respectively. Adding electrons/holes by electrostatic gating further reveals abundant emission features associated with charged exciton species whose multiparticle nature and spin/valley configuration have attracted much recent interest.[28−33] In this work, we focus on the hole doping regime. As holes are introduced into the device, BX rapidly diminishes, while the interaction of the exciton with the hole Fermi Sea results in two repelling branches of exciton polarons: X^+ the attractive polaron, and X the repulsive polaron.[9,34−37] Figure 1b left panel shows detailed spectral

https://doi.org/10.1021/acsnano.3c02737
ACS Nano 2023, 17, 15641−15647

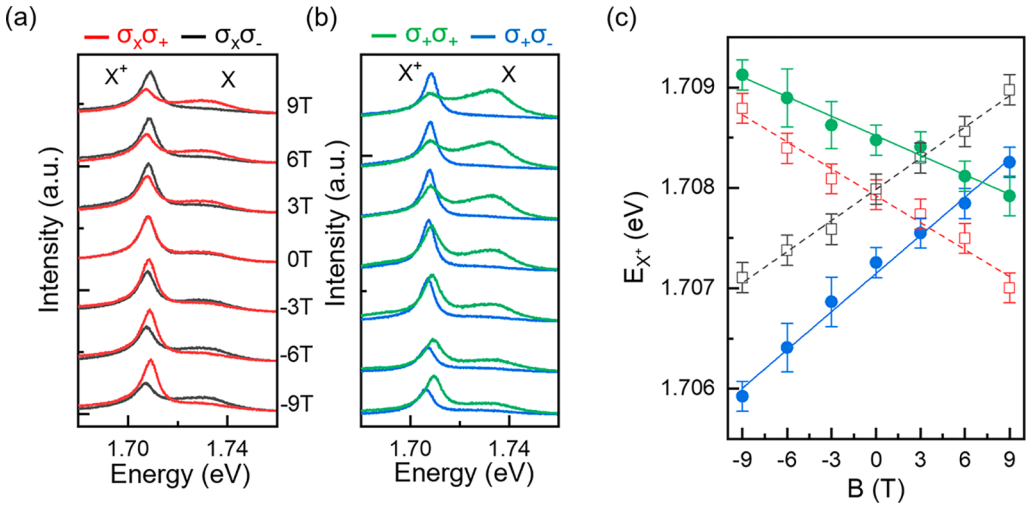

Figure 3. Magnetic field dependent circular polarization resolved photoluminescence with (a) linearly and (b) circularly polarized excitation. The energy of X^+ from −9 T to 9 T is plotted in (c) for $\sigma_x\sigma_-$ (black squares), $\sigma_x\sigma_+$ (red squares), $\sigma_x\sigma_-$ (blue circles), $\sigma_+\sigma_+$ (green circles) polarizations.

evolution under linearly polarized optical excitation and detection. With the filling of the hole Fermi sea, the spectral weight of the X polaron is gradually transferred to the X^+ polaron. The spectral lineshapes in the two detection channels are similar, and the small difference in intensity reflects finite valley coherence induced by the linearly polarized excitation that populates a coherent superposition of K and −K valley excitons.

The circular polarization resolved spectra in the Figure 1b right panel are drastically different. While at low doping where X and X^+ polarons can be viewed as excitons and trions, respectively, the spectral lineshapes in the σ_+ (green) and σ_- (blue) channels are similar, at high doping levels the lineshapes become very different: compared to σ_-, the σ_+ emission channel has a much larger spectral weight in the X branch. From the valley optical selection rule,[38] the σ_+ and σ_- emissions correspond to radiative recombination of bright excitonic species in K and −K valleys, respectively. Our data thus point to very different valley polarization for X and X^+ polarons. As quantitatively plotted in Figure 1c, the X polaron valley polarization becomes very high as holes are introduced into the atomic layer. The behavior of X^+ is also very interesting: its smaller valley polarization (Figure 1c, right axis) is accompanied by a striking splitting of the attractive polaron energy in the σ_+ and σ_- emission channels.

The time-reversal-symmetry breaking effects for the K and −K valley exciton polarons in Figure 1b right panel are induced by valley polarized optical injection with σ_+ optical excitation. Figure 2 shows the spectral evolution of K and −K valley exciton polarons as a function of laser illumination power at several representative hole doping levels. At low laser intensity the spectra appear "normal", similar to linearly polarized data in Figure 1b, with the energy of polarons degenerate in the two valleys and similar X and X^+ valley polarization. As the laser intensity increases, more and more spectral weight is transferred from X^+ to X in the σ_+ emission channel (K valley). This leads to a decrease of valley polarization for the X^+ polaron concomitant with the emergence of a valley splitting for polaron energy, as plotted in Figure 2b. The valley polarization of the repulsive polaron X also significantly improves, most obviously seen from data with a hole density at 1.2×10^{12} cm^{-2}. Meanwhile the X^+ polaron line width becomes wider in $\sigma_+\sigma_+$ than in $\sigma_+\sigma_-$ as the laser power increases. This broadening could be related to the electron-recoil effect,[39] exciton-induced scattering dephasing,[40] and screening from potential fluctuations.[36]

The size of the X^+ polaron valley splitting is comparable to valley splitting induced by an external magnetic field of a few Tesla. In Figure 3 (device D2, see Supporting Information for device D1), we tune the valley exciton polarons populated by linearly or circularly polarized optical excitations with an external magnetic field. For linear excitation in Figure 3a, the σ_+ and σ_- spectra almost overlap at 0 T, reflecting the same population of attractive and repulsive polarons in the two valleys. When the magnetic field is finite, the valley degeneracy is lifted, and the spectral weight distribution between attractive and repulsive polarons becomes different for polarons residing in the two valleys. Since K and −K valleys form a time-reversal pair, we observe in Figure 3a an "antisymmetric" behavior with respect to the zero magnetic field: σ_+ spectra in a positive field behave like the σ_- spectra in a negative field. This antisymmetry is broken for data in Figure 3b where circularly polarized optical excitation is used, and we observe more intense X repulsive polaron emission in the σ_+ channel in the entire field range. The energy splitting for X^+ attractive polaron is also not antisymmetric with respect to the 0 magnetic field. Figure 3c shows the energy evolution of attractive exciton polarons. Under linear excitation the K and −K polaron energies cross at 0 field as expected. For circular excitation, however, the crossing occurs at about 7 T.

Discussion. How do we understand the peculiar behaviors of exciton polarons under circular excitation? Did the circularly polarized light act as an effective magnetic field of −7 T in our device? Circularly polarized optical excitation is known to be capable of generating a pseudomagnetic field in TMD semiconductors via the optical Stark effect, where intense subgap optical pulses hybridize with the excitonic mode in one valley but not the other, shifting the exciton energy and lifting the valley degeneracy.[19,20] In our study here, the experimental conditions are quite different from those in refs 19 and 20. Our optical excitation is a continuous wave at sub-mW power, which is orders of magnitude less intense. Further, our

https://doi.org/10.1021/acsnano.3c02737
ACS Nano 2023, 17, 15641−15647

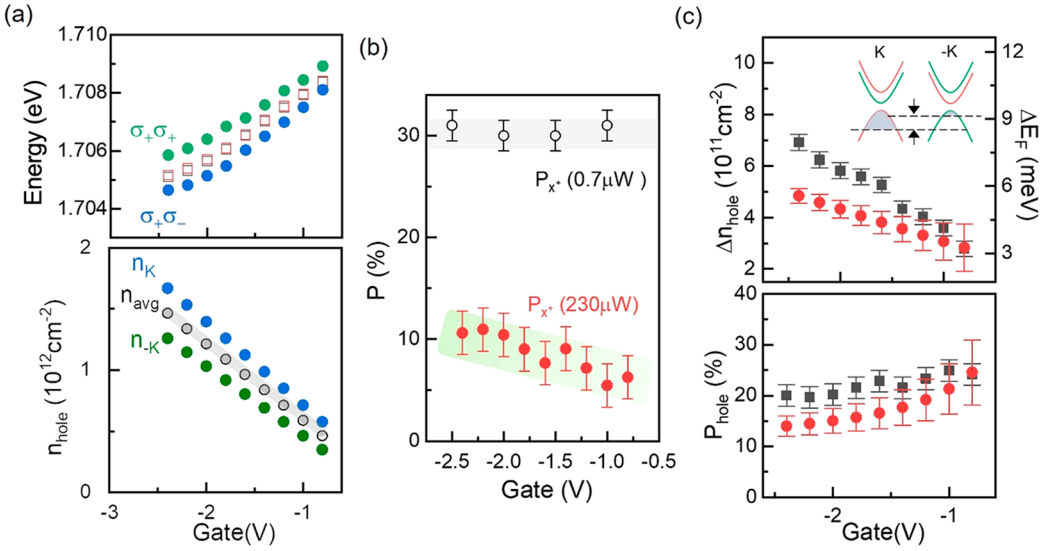

Figure 4. (a) Top: gate voltage dependent energy shift of X^+ with linearly polarized excitation (open symbols) and circularly polarized σ_+ excitation (filled symbols). Bottom: the extracted hole concentrations in the K valley (blue), −K valley (green), and average (black) under σ_+ excitation. The gray line shows the expected average carrier density with the geometric capacitance model. (b) The polarization of X^+ at low (0.7 μW, gray) and high (230 μW, red) excitation power under circularly polarized excitations at different gate voltages. (c) Top: the estimated difference of hole density between the two valleys by using energy splitting (red) and valley polarization (black) of X^+. Bottom: the corresponding valley polarization of resident holes.

excitation is above the optical bandgap, and tuning the incident photon energy over a wide range does not have much impact on the size of the polaron valley splitting (see Supporting Information). This is in contrast to the optical Stark effect where the energy splitting between the two valleys is highly sensitive to how much the photon energy is detuned from the optical bandgap.[19,20] We thus rule out the optical stark effect playing a role in our observations. In the following, we explain our experimental observations as due to an imbalanced valley population of mobile holes produced by circularly polarized optical excitation. As illustrated in Figure 2c, the optically excited electrons in the K valley can make a spin-conserved transition to the −K valley. This process is presumably more efficient than intervalley scattering of holes, which requires a spin-flip due to the large spin−orbital splitting (~0.5 eV) in the valence band. An excess of mobile holes is thus expected in the K valley as illustrated in Figure 2d due to valley injection of excitons. We note that this physics picture of more efficient spin-preserved intervalley scatterings over spin-flipped intervalley processes during relaxation of energetic carriers is compatible with previous investigations of resident charges generated by pulsed or cw laser excitations.[21−27]

To understand the impact of valley imbalanced holes on the exciton polaron spectra, we first revisit the magnetic field dependence data in Figure 3a for the hole doped device under linear optical excitation, where such an imbalance is caused by the Zeeman shift of the valence bands. For the red σ_+ emission from radiative recombination of electrons and holes in the K valley, we observe that the X^+ polaron loses intensity as the magnetic field increases from 0 to positive values, while the broader X emission gains intensity. Considering the energies of the Zeeman split polarons, it appears a bit strange that at 9 T the −K valley X^+ polaron (σ_- black spectrum) is more intense than the red +K valley X^+ polaron since the latter is energetically more favorable to populate. In fact, at 9 T both X and X^+ polarons in the +K valley should have lower energy,[12−15] and yet X^+ is less intense while X is more intense than their corresponding species in the −K valley. We thus conclude that the emission intensities are not determined by the thermal distribution of the excitonic species. Instead, the more important factor to consider here is the density of holes in the two valleys, which are imbalanced by the magnetic field.

In the low-density limit of hole doping, the repulsive and attractive polarons reduce to excitons and positive trions, respectively. It has been established that in a positive trion, the two holes do not reside in the same valley which would otherwise result in an excessively large exchange energy.[9,34,41] As we dope the device with more holes that form a Fermi sea, excitons in one valley are dominantly dressed by the Fermi sea in the opposite valley, where the resident holes have opposite spin. This dressing has a prominent impact on the spectral weight distribution between attractive and repulsive polarons.[9] For our experiment in Figure 3a under positive magnetic fields, the K (−K) valley valence band shifts up (down). Thus, hole density increases in the K valley and decreases in the −K valley. As a result, the −K valley polarons distribute more spectral weight to the X^+ attractive branch than K valley polarons do. This explains why in Figure 3a the X and X^+ polaron emissions exhibit opposite valley polarization trends as the magnetic field is tuned.

Given the above physics picture, our circular polarization resolved data in Figure 1b are consistent with the scenario where σ_+ polarized light injects holes into the +K valley (Figure 2c). Note that the total density of charges in the device is determined by the gate voltage; an increase of hole density in the K valley leads to a corresponding decrease in the −K valley (Figure 2d): an imbalance that indeed mimics the impact of an external magnetic field, except that here there is no valence band energy shift and that the chemical potential difference in the two valleys is maintained by a steady source of valley polarized holes supplied by circularly polarized optical excitation. In this scenario, under σ_+ excitation, a more rapid decrease of X intensity in the −K valley ($\sigma_+\sigma_-$ spectra in Figure 1b), compared to data under linear excitation, is compatible

https://doi.org/10.1021/acsnano.3c02737
ACS Nano 2023, 17, 15641−15647

with a larger Fermi sea in the K valley due to the intervalley nature of the exciton-charge dressing effects. Similarly, the decrease of X spectral weight in the K valley ($\sigma_+\sigma_+$ spectra in Figure 1b) is more gradual compared to linear excitation since a portion of the holes are depleted from the −K valley. This opposite trend in the two valleys leads to a very large valley polarization for the X mode at relatively high hole doping (Figure 1c). It also explains why the valley polarization of X^+ is much smaller compared to that of X polarons.

Dressing of excitons with charges leads to a red-shift of the X^+ polaron mode. The imbalanced population of holes in the two valleys provides a natural explanation for the energy splitting of the X^+ exciton-polarons under σ_+ illumination in the Figure 1b right panel. In the upper panel of Figure 4a we quantitatively plot the polaron energies as a function of gate voltage. The open symbols are extracted from data in Figure 1b under linear excitation, where K and −K valleys have the same hole density. Data (filled symbols) extracted from circularly polarized spectra lie above ($\sigma_+\sigma_+$) and below ($\sigma_+\sigma_-$) the open symbols, respectively, reflecting a smaller Fermi sea in the −K valley than in K. The average charge density in the device can be obtained by considering the gate geometry. With an hBN thickness of 18 nm between the graphene gate and WSe_2, 1.2×10^{12} cm^{-2} holes are injected per volt of gate tuning (Figure 2a lower panel gray line). The open symbols in the upper panel of Figure 4a provide a calibration for the attractive polaron energy shift with respect to hole density. This allows us to extract the hole density in K and −K valleys separately under circular optical excitation. In Figure 4a lower panel, we plot the hole density in the two valleys (blue filled: K, green filled: −K), as well as their average n_{avg} (open symbols), which agrees well with the geometric capacitance model (line). The hole density difference for the two valleys varies between 2 and 5×10^{11} cm^{-2} from low to high gate voltages, which we plot as red dots in the Figure 4c upper panel. Defining the valley polarization of holes as $P_h = \frac{n_K - n_{-K}}{n_K + n_{-K}}$, we find P_h varies between 13% and 25% in our device depending on the gate voltage (red symbols in Figure 4c lower panel). Assuming a hole mass of $0.5m_e$, the hole density difference can also be expressed as the Fermi energy difference in the two valleys. As shown in Figure 4c upper panel right axis, the Fermi level difference between the two valleys gets as high as 5 meV. As a comparison, to induce such a Fermi energy valley contrast with the Zeeman effect, a magnetic field as high as ∼7 T needs to be applied. We note that in $WSe_2/MoSe_2$ heterojunctions interlayer excitons in the two valleys can also acquire an energy splitting when excited by circularly polarized cw laser excitations. Interestingly, two works[42,43] found opposite shifts for the copolarized emission, and they were interpreted with different mechanisms, one with Coulomb repulsion between holes and the other with exchange interaction between excitons. For the former, the copolarized emission acquires a red-shift, opposite to our exciton polaron, although the generation of valley imbalanced holes resembles our process in Figure 2c. For the latter, the copolarized emission acquires a blue-shift, similar to our exciton polaron, but the mechanism is completely different. We also note that in the latter case the magnetic field required to bring the excitons back to degeneracy is comparable to ours.

The value of the X^+ attractive polaron valley polarization plotted in Figure 4b provides additional insight into the hole density imbalance between the two valleys. At low levels of optical excitation (0.7 μW), the valley polarization of X^+ is ∼0.3, similar to X. The diminished valley polarization of X^+ observed in Figure 2 as the laser intensity increases can be viewed as a competition between initial optical population of valley polarized excitons and the eventual valley imbalanced injection of resident holes. Following ref 27, we model the X^+ polarization as $P_{X^+} = \frac{P_0 - P_h}{1 - P_0 P_h}$, where P_0 is the initial valley polarization in the low illumination limit. Using the valley polarization data in Figure 4b at high optical illumination (230 μW), we extract P_h plotted as black symbols in the Figure 4c lower panel. The two methods give similar valley polarization for holes. We also plotted as black symbols in Figure 4c top panel the hole density difference between the two valleys to compare it with red dots extracted from exciton polaron energy splitting.

We finally comment that the spectroscopic splitting due to circularly polarized optical injection of resident charges offers an interesting perspective into the exciton polaron energy shift under the impact of an external magnetic field. This energy shift, such as those in Figure 3a, is usually interpreted as the Zeeman effect on the magnetic dipole moment of excitons. However, for a doped device, the magnetic field also creates imbalanced charge density in the two valleys,[44] which would lead to another field-dependent energy shift contribution due to intervalley exciton polaron dressing. In Figure 5a, we show

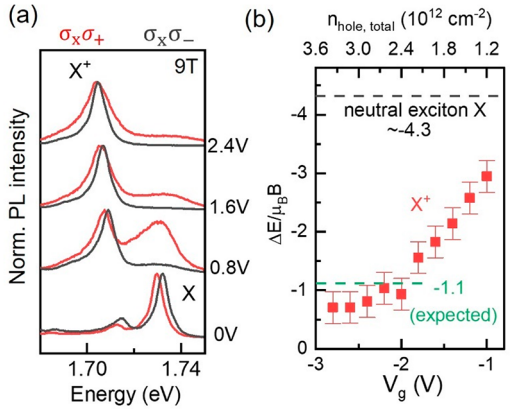

Figure 5. (a) Gate voltage dependent photoluminescence of 1L-WSe_2 at 9 T from K ($\sigma_x\sigma_+$) and −K ($\sigma_x\sigma_-$) valleys. Spectra intensities are normalized to highlight the energy separation between σ_+ and σ_- emission channels. (b) The energy splitting of X^+ at various doping levels, with the black dashed line showing splitting of neutral exciton X and the green dashed line indicating the expected energy splitting taking into account both the Zeeman shift of valence band and exciton polaron dressing for X^+.

at 9 T the circular polarization resolved polaron spectra evolution at several hole doping levels. The energy splitting for X^+ between the two valleys, $\Delta E = E_K - E_{-K}$, normalized by $\mu_B B$, diminishes when more holes are introduced and eventually saturates at around −0.8 at high doping levels, as shown in Figure 5b. The valence band g factor has a measured value of 6.1.[45] Thus, at 9 T and large hole doping, the Fermi energy difference of the two valleys is about 6 meV. Making use of exciton polaron energy shift vs Fermi energy in Figure 4a, we assess a reduced splitting of −1.1 $\mu_B B$. This is represented as the dashed green line in Figure 5b, which is in reasonable agreement with our experimental data.

https://doi.org/10.1021/acsnano.3c02737
ACS Nano 2023, 17, 15641−15647

CONCLUSIONS

In conclusion, we demonstrate light-induced energy splitting and valley polarization of exciton-polarons in monolayer WSe_2 as a result of the imbalanced buildup of holes residing in two opposite valleys. The splitting in energy and the valley polarization provide an estimation of density of light-induced valley polarized holes approaching several 10^{11} cm^{-2} with an equivalent Fermi level difference reaching around 5 meV among valleys. This quantitative understanding is essential for optical valleytronic applications using monolayer TMDs and provides insight for understanding spin-valley properties of TMD structures.

METHODS

Crystal Growth. The bulk WSe_2 crystals are grown by the chemical vapor transport (CVT) method. High purity W 99.99%, Se 99.999%, and I_2 99.99% (Sigma-Aldrich) are placed in a fused silica tubing that is 300 mm long with an internal diameter of 18 mm. W and Se are kept in a 1:2 stoichiometric ratio with a total mass of 2 g. Sufficient I_2 is added to achieve a density of 10 mg cm^{-3}. The tube is pump-purged with argon gas (99.999%) at least five times and sealed at low pressure prior to growth. Using a three-zone furnace, the reaction and growth zones are set to 1055 and 955 °C, respectively. The growth time was approximately 2 weeks.

Sample Fabrication. The atomic flakes of WSe_2, hexagonal boron nitride (hBN), and graphene are first exfoliated on Si wafers with 300 nm of SiO_2 and inspected under an optical microscope. To make high quality 1L-WSe_2 heterostructures, we annealed hBN in an O_2/Ar atmosphere (50 sccm/200 sccm) at 500 °C for 2−3 h before stacking. The flakes are then stacked with a few-layer graphene flake as the back gate and transferred to substrates with premade electrodes using a dry transfer technique with a polypropylene carbonate (PPC) stamp. All the exfoliation, inspection, and stacking processes are completed in a glovebox with controlled humidity and oxygen both <0.01 ppm to minimize sample degradation. The stacked samples are thermally annealed at 350 °C for 1 h in an argon environment to improve the quality.

Photoluminescence Spectroscopy. The sample is transferred to a closed loop cryostat with optical access. A He−Ne 633 nm (1.959 eV) laser is used for optical excitation. All measurements in this work are performed at 3.4 K. The incident laser is reflected by a nonpolarizing cube beam splitter and then focused on the sample by a 50× objective lens (NA: 0.35) with a spot size of ∼2 μm. The polarization of the incident beam is controlled by a linear polarizer and a quarter-waveplate on the incident optical path, while the polarization resolved collection is achieved with a polarization analyzer set in the collection path. The sample emission is guided into a Horiba T64000 spectrometer equipped with a liquid nitrogen cooled CCD.

ASSOCIATED CONTENT

Supporting Information

The Supporting Information is available free of charge at https://pubs.acs.org/doi/10.1021/acsnano.3c02737.

Additional data from devices D1 and D2, detuned excitations, circularly polarized (σ_+ and σ_-) excitations, circular polarization analysis (PDF)

AUTHOR INFORMATION

Corresponding Author

Jun Yan − *Department of Physics, University of Massachusetts Amherst, Amherst, Massachusetts 01003, United States;* orcid.org/0000-0003-3861-4633; Email: yan@physics.umass.edu

Authors

Yueh-Chun Wu − *Department of Physics, University of Massachusetts Amherst, Amherst, Massachusetts 01003, United States;* orcid.org/0000-0002-9299-6882

Takashi Taniguchi − *International Center for Materials Nanoarchitectonics, National Institute for Materials Science, Tsukuba, Ibaraki 305-0044, Japan;* orcid.org/0000-0002-1467-3105

Kenji Watanabe − *Research Center for Functional Materials, National Institute for Materials Science, Tsukuba, Ibaraki 305-0044, Japan;* orcid.org/0000-0003-3701-8119

Complete contact information is available at: https://pubs.acs.org/10.1021/acsnano.3c02737

Notes

The authors declare no competing financial interest.

ACKNOWLEDGMENTS

This work is supported by the National Science Foundation (DMR-2004474). K.W. and T.T. acknowledge support from JSPS KAKENHI (Grant Numbers 19H05790, 20H00354, and 21H05233).

REFERENCES

(1) Xu, X.; Yao, W.; Xiao, D.; Heinz, T. F. Spin and Pseudospins in Layered Transition Metal Dichalcogenides. *Nat. Phys.* **2014**, *10*, 343−350.

(2) Zeng, H.; Dai, J.; Yao, W.; Xiao, D.; Cui, X. Valley Polarization in MoS_2 Monolayers by Optical Pumping. *Nature Nanotechnology.* **2012**, *7*, 490−493.

(3) Mak, K. F.; He, K.; Shan, J.; Heinz, T. F. Control of Valley Polarization in Monolayer MoS_2 by Optical Helicity. *Nature Nanotechnology.* **2012**, *7*, 494−498.

(4) Cao, T.; Wang, G.; Han, W.; Ye, H.; Zhu, C.; Shi, J.; Niu, Q.; Tan, P.; Wang, E.; Liu, B.; Feng, J. Valley-Selective Circular Dichroism of Monolayer Molybdenum Disulphide. *Nat. Commun.* **2012**, *3*, 887.

(5) Rivera, P.; Seyler, K. L.; Yu, H.; Schaibley, J. R.; Yan, J.; Mandrus, D. G.; Yao, W.; Xu, X. Valley-Polarized Exciton Dynamics in a 2D Semiconductor Heterostructure. *Science* **2016**, *351*, 688−691.

(6) Wang, G.; Palleau, E.; Amand, T.; Tongay, S.; Marie, X.; Urbaszek, B. Polarization and Time-Resolved Photoluminescence Spectroscopy of Excitons in $MoSe_2$ Monolayers. *Appl. Phys. Lett.* **2015**, *106*, 112101.

(7) Chen, S.-Y.; Goldstein, T.; Tong, J.; Taniguchi, T.; Watanabe, K.; Yan, J. Superior Valley Polarization and Coherence of 2s Excitons in Monolayer WSe_2. *Phys. Rev. Lett.* **2018**, *120*, 046402.

(8) Shinokita, K.; Wang, X.; Miyauchi, Y.; Watanabe, K.; Taniguchi, T.; Matsuda, K. Continuous Control and Enhancement of Excitonic Valley Polarization in Monolayer WSe_2 by Electrostatic Doping. *Adv. Funct. Mater.* **2019**, *29*, 1900260.

(9) Wu, Y.-C.; Taniguchi, T.; Watanabe, K.; Yan, J. Negative Valley Polarization in Doped Monolayer $MoSe_2$. *Phys. Chem. Chem. Phys.* **2021**, *24*, 191−196.

(10) Wu, Y. C.; Taniguchi, T.; Watanabe, K.; Yan, J. Enhancement of Exciton Valley Polarization in Monolayer Induced by Scattering. *Phys. Rev. B* **2021**, *104*, L121408.

(11) Jiang, C.; Xu, W.; Rasmita, A.; Huang, Z.; Li, K.; Xiong, Q.; Gao, W. Microsecond Dark-Exciton Valley Polarization Memory in Two-Dimensional Heterostructures. *Nat. Commun.* **2018**, *9*, 753.

(12) Aivazian, G.; Gong, Z.; Jones, A. M.; Chu, R.-L.; Yan, J.; Mandrus, D. G.; Zhang, C.; Cobden, D.; Yao, W.; Xu, X. Magnetic Control of Valley Pseudospin in Monolayer WSe_2. *Nat. Phys.* **2015**, *11*, 148−152.

(13) Srivastava, A.; Sidler, M.; Allain, A. V.; Lembke, D. S.; Kis, A.; Imamoğlu, A. Valley Zeeman Effect in Elementary Optical Excitations of Monolayer WSe_2. *Nat. Phys.* **2015**, *11*, 141−147.
(14) MacNeill, D.; Heikes, C.; Mak, K. F.; Anderson, Z.; Kormányos, A.; Zólyomi, V.; Park, J.; Ralph, D. C. Breaking of Valley Degeneracy by Magnetic Field in Monolayer $MoSe_2$. *Phys. Rev. Lett.* **2015**, *114*, 037401.
(15) Li, Y.; Ludwig, J.; Low, T.; Chernikov, A.; Cui, X.; Arefe, G.; Kim, Y. D.; van der Zande, A. M.; Rigosi, A.; Hill, H. M.; Kim, S. H.; Hone, J.; Li, Z.; Smirnov, D.; Heinz, T. F. Valley Splitting and Polarization by the Zeeman Effect in Monolayer $MoSe_2$. *Phys. Rev. Lett.* **2014**, *113*, 266804.
(16) Lu, Z.; Rhodes, D.; Li, Z.; Van Tuan, D.; Jiang, Y.; Ludwig, J.; Jiang, Z.; Lian, Z.; Shi, S.-F.; Hone, J.; Dery, H.; Smirnov, D. Magnetic Field Mixing and Splitting of Bright and Dark Excitons in Monolayer $MoSe_2$. *2D Mater.* **2020**, *7*, 015017.
(17) Chen, S.-Y.; Lu, Z.; Goldstein, T.; Tong, J.; Chaves, A.; Kunstmann, J.; Cavalcante, L. S. R.; Woźniak, T.; Seifert, G.; Reichman, D. R.; Taniguchi, T.; Watanabe, K.; Smirnov, D.; Yan, J. Luminescent Emission of Excited Rydberg Excitons from Monolayer WSe_2. *Nano Lett.* **2019**, *19*, 2464−2471.
(18) Goryca, M.; Li, J.; Stier, A. V.; Taniguchi, T.; Watanabe, K.; Courtade, E.; Shree, S.; Robert, C.; Urbaszek, B.; Marie, X.; Crooker, S. A. Revealing Exciton Masses and Dielectric Properties of Monolayer Semiconductors with High Magnetic Fields. *Nat. Commun.* **2019**, *10*, 4172.
(19) Kim, J.; Hong, X.; Jin, C.; Shi, S.-F.; Chang, C.-Y. S.; Chiu, M.-H.; Li, L.-J.; Wang, F. Ultrafast Generation of Pseudo-Magnetic Field for Valley Excitons in WSe_2 Monolayers. *Science* **2014**, *346*, 1205−1208.
(20) Sie, E. J.; McIver, J. W.; Lee, Y.-H.; Fu, L.; Kong, J.; Gedik, N. Valley-Selective Optical Stark Effect in Monolayer WS_2. *Nat. Mater.* **2015**, *14*, 290−294.
(21) Yang, L.; Sinitsyn, N. A.; Chen, W.; Yuan, J.; Zhang, J.; Lou, J.; Crooker, S. A. Long-Lived Nanosecond Spin Relaxation and Spin Coherence of Electrons in Monolayer MoS_2 and WS_2. *Nat. Phys.* **2015**, *11*, 830−834.
(22) Hsu, W. T.; Chen, Y. L.; Chen, C. H.; Liu, P. S.; Hou, T. H.; Li, L. J.; Chang, W. H. Optically Initialized Robust Valley-Polarized Holes in Monolayer WSe_2. *Nat. Commun.* **2015**, *6*, 8963.
(23) Song, X.; Xie, S.; Kang, K.; Park, J.; Sih, V. Long-Lived Hole Spin/Valley Polarization Probed by Kerr Rotation in Monolayer WSe_2. *Nano Lett.* **2016**, *16*, 5010−5014.
(24) Dey, P.; Yang, L.; Robert, C.; Wang, G.; Urbaszek, B.; Marie, X.; Crooker, S. A. Gate-Controlled Spin-Valley Locking of Resident Carriers in WSe_2 Monolayers. *Phys. Rev. Lett.* **2017**, *119*, 137401.
(25) Li, J.; Goryca, M.; Yumigeta, K.; Li, H.; Tongay, S.; Crooker, S. A. Valley Relaxation of Resident Electrons and Holes in a Monolayer Semiconductor: Dependence on Carrier Density and the Role of Substrate-Induced Disorder. *Phys. Rev. Mater.* **2021**, *5*, 044001.
(26) Ersfeld, M.; Volmer, F.; Rathmann, L.; Kotewitz, L.; Heithoff, M.; Lohmann, M.; Yang, B.; Watanabe, K.; Taniguchi, T.; Bartels, L.; Shi, J.; Stampfer, C.; Beschoten, B. Unveiling Valley Lifetimes of Free Charge Carriers in Monolayer WSe_2. *Nano Lett.* **2020**, *20*, 3147−3154.
(27) Robert, C.; Park, S.; Cadiz, F.; Lombez, L.; Ren, L.; Tornatzky, H.; Rowe, A.; Paget, D.; Sirotti, F.; Yang, M.; Van Tuan, D.; Taniguchi, T.; Urbaszek, B.; Watanabe, K.; Amand, T.; Dery, H.; Marie, X. Spin/Valley Pumping of Resident Electrons in WSe_2 and WS_2 Monolayers. *Nat. Commun.* **2021**, *12*, 5455.
(28) Van Tuan, D.; Shi, S.-F.; Xu, X.; Crooker, S. A.; Dery, H. Six-Body and Eight-Body Exciton States in Monolayer WSe_2. *Phys. Rev. Lett.* **2022**, *129*, 76801.
(29) Wu, Y.-C.; Samudrala, S.; McClung, A.; Taniguchi, T.; Watanabe, K.; Arbabi, A.; Yan, J. Up- and Down-Conversion between Intra- and Intervalley Excitons in Waveguide Coupled Monolayer WSe_2. *ACS Nano* **2020**, *14*, 10503.
(30) Liu, E.; Van Baren, J.; Lu, Z.; Altaiary, M. M.; Taniguchi, T.; Watanabe, K.; Smirnov, D.; Lui, C. H. Gate Tunable Dark Trions in Monolayer WSe_2. *Phys. Rev. Lett.* **2019**, *123*, 027401.
(31) Chen, S.-Y.; Goldstein, T.; Taniguchi, T.; Watanabe, K.; Yan, J. Coulomb-Bound Four- and Five-Particle Intervalley States in an Atomically-Thin Semiconductor. *Nat. Commun.* **2018**, *9*, 3717.
(32) Hao, K.; Specht, J. F.; Nagler, P.; Xu, L.; Tran, K.; Singh, A.; Dass, C. K.; Schüller, C.; Korn, T.; Richter, M.; Knorr, A.; Li, X.; Moody, G. Neutral and Charged Inter-Valley Biexcitons in Monolayer $MoSe_2$. *Nat. Commun.* **2017**, *8*, 15552.
(33) He, M.; Rivera, P.; Van Tuan, D.; Wilson, N. P.; Yang, M.; Taniguchi, T.; Watanabe, K.; Yan, J.; Mandrus, D. G.; Yu, H.; Dery, H.; Yao, W.; Xu, X. Valley Phonons and Exciton Complexes in a Monolayer Semiconductor. *Nat. Commun.* **2020**, *11*, 618.
(34) Efimkin, D. K.; MacDonald, A. H. Many-Body Theory of Trion Absorption Features in Two-Dimensional Semiconductors. *Phys. Rev. B* **2017**, *95*, 035417.
(35) Efimkin, D. K.; MacDonald, A. H. Exciton-Polarons in Doped Semiconductors in a Strong Magnetic Field. *Phys. Rev. B* **2018**, *97*, 235432.
(36) Goldstein, T.; Wu, Y.-C.; Chen, S.-Y.; Taniguchi, T.; Watanabe, K.; Varga, K.; Yan, J. Ground and Excited State Exciton Polarons in Monolayer $MoSe_2$. *J. Chem. Phys.* **2020**, *153*, 071101.
(37) Liu, E.; van Baren, J.; Lu, Z.; Taniguchi, T.; Watanabe, K.; Smirnov, D.; Chang, Y.-C.; Lui, C. H. Exciton-Polaron Rydberg States in Monolayer $MoSe_2$ and WSe_2. *Nat. Commun.* **2021**, *12*, 6131.
(38) Xiao, D.; Liu, G.; Feng, W.; Xu, X.; Yao, W. Coupled Spin and Valley Physics in Monolayers of MoS_2 and Other Group-VI Dichalcogenides. *Phys. Rev. Lett.* **2012**, *108*, 196802.
(39) Zipfel, J.; Wagner, K.; Semina, M. A.; Ziegler, J. D.; Taniguchi, T.; Watanabe, K.; Glazov, M. M.; Chernikov, A. Electron Recoil Effect in Electrically Tunable $MoSe_2$ Monolayers. *Phys. Rev. B* **2022**, *105*, 75311.
(40) Katsch, F.; Selig, M.; Knorr, A. Exciton-Scattering-Induced Dephasing in Two-Dimensional Semiconductors. *Phys. Rev. Lett.* **2020**, *124*, 257402.
(41) Yu, H.; Liu, G.-B.; Gong, P.; Xu, X.; Yao, W. Dirac Cones and Dirac Saddle Points of Bright Excitons in Monolayer Transition Metal Dichalcogenides. *Nat. Commun.* **2014**, *5*, 3876.
(42) Li, W.; Lu, X.; Wu, J.; Srivastava, A. Optical Control of the Valley Zeeman Effect through Many-Exciton Interactions. *Nat. Nanotechnol.* **2021**, *16*, 148−152.
(43) Jiang, C.; Rasmita, A.; Xu, W.; Imamoğlu, A.; Xiong, Q.; Gao, W. Optical Spin Pumping Induced Pseudomagnetic Field in Two-Dimensional Heterostructures. *Phys. Rev. B* **2018**, *98*, 241410.
(44) Glazov, M. M. Optical Properties of Charged Excitons in Two-Dimensional Semiconductors. *J. Chem. Phys.* **2020**, *153*, 034703.
(45) Robert, C.; Dery, H.; Ren, L.; Van Tuan, D.; Courtade, E.; Yang, M.; Urbaszek, B.; Lagarde, D.; Watanabe, K.; Taniguchi, T.; Amand, T.; Marie, X. Measurement of Conduction and Valence Bands G-Factors in a Transition Metal Dichalcogenide Monolayer. *Phys. Rev. Lett.* **2021**, *126*, 067403.

https://doi.org/10.1021/acsnano.3c02737
ACS Nano 2023, 17, 15641−15647